Available online at www.sciencedirect.com

SciVerse ScienceDirect

Ceramics International 38 (2012) 1409–1416

CERAMICS INTERNATIONAL

www.elsevier.com/locate/ceramint

The comparison of mechanical behavior of $MgO–MgAl_2O_4$ with $MgO–ZrO_2$ and $MgO–MgAl_2O_4–ZrSiO_4$ composite refractories

Rasim Ceylantekin [a,*], Cemail Aksel [b]

[a] Dumlupınar University, Dept. of Ceramics Eng., Kütahya 43100, Turkey
[b] Anadolu University, Dept. of Mats. Scien. Eng., Eskişehir 26030, Turkey

Received 12 August 2011; received in revised form 5 September 2011; accepted 6 September 2011
Available online 14 September 2011

Abstract

Mechanical properties of different compositions obtained from the additions of 5, 10, 20 and 30 wt.% zircon ($ZrSiO_4$) into the MgO–spinel composite refractories and ZrO_2 into MgO have been examined, the variations that occurred have been determined, and the parameters affecting those factors have been investigated with the reasons. The density, strength, Young's modulus, fracture toughness, fracture surface energy and work of fracture were measured and evaluated. Microstructural variations and fracture surfaces have been examined and the formation of new phases has been identified depending on the additive type and quantity. The relationships between mechanical properties and structural variations for different compositions have been examined. In MgO–spinel materials, strength, Young's modulus and fracture toughness values decrease up to 20% spinel addition and stay almost constant for further loads. ZrO_2 addition displays same trend but not as effective as spinel. Besides, since ZrO_2 is stable in cubic form, it does not show any toughening mechanism. Forsterite formation is the most important factor for 2-fold improvement in the mechanical properties of MgO–spinel–zircon refractories. The more the zircon addition, the more the mechanical properties improve. The generation of natural bonding between matrix particles with forsterite formation, on the other hand, causes the fracture path to turn to transgranular fracture with an increase in fracture surface energy and a decrease in work of fracture, among which the latter is considered as an indicator of thermal shock resistance of the materials being high.

Keywords: C. Mechanical properties; D. MgO; D. Spinels; D. ZrO_2; Zircon; Refractory

1. Introduction

Magnesia–chromite ($MgO–Cr_2O_3$) bricks have been used as standard lining for the hot kiln zones since 1940. Their properties, e.g. thermal conductivity, thermal shock resistance and thermal expansion, mainly depend on the refractory grade chrome ores [1]. However, because of the risk of contamination of ground water by $Cr^{[VI]}$ ions leaching from waste refractory materials, and because $Cr^{[VI]}$ has in particular been associated with allergic skin ulceration and carcinomas, the replacement of the chrome in these refractories has become a challenge [2–4]. For this reason, attention has been given to the use of magnesium aluminate spinel, $MgAl_2O_4$, as an alternative to chrome ore [5–7]. While magnesite is often used alone, magnesium aluminate spinel is now widely incorporated in magnesite-based refractories [8,9]. A further major advantage of the magnesite–spinel refractories is that they have improved thermal shock resistance, and it is claimed that two to three times longer service life can be obtained, compared to a conventional magnesite–chrome brick [10,11].

The optimum spinel content, reported so far, is variable depending on the properties of spinel. Cooper and Hudson [12] found 40 wt.% spinel refractories exhibited the best combination of properties with superior resistance against thermal shock while Aksel and Riley [13] reported 20 wt.% was sufficient.

While service life of refractories is prolonged especially in connection with the increase in work of fracture energy by addition of spinel particles to MgO, a reduction occurs in other mechanical properties [5,6].

This study has been conducted for further improving the mechanical performances of materials and further prolonging service life by deriving high thermomechanical properties as a result of the increase in resistance to fracture by addition of zircon ($ZrSiO_4$) in different proportions to MgO–spinel

* Corresponding author. Tel.: +90 274 265 20 31; fax: +90 274 265 20 66.
E-mail addresses: rceylantekin@dpu.edu.tr, rceylantekin@anadolu.edu.tr (R. Ceylantekin).

0272-8842/$36.00
doi:10.1016/j.ceramint.2011.09.020

composite refractories containing various quantities of spinel ($MgAl_2O_4$) and ZrO_2 to MgO. The relationships between mechanisms affording improvement in the mechanical behaviors of refractories and microstructural changes and parameters affecting these have been analyzed in detail.

2. Experimental

Recipes were prepared by adding ZrO_2 in proportion of 5%, 10%, 20% and 30% to MgO (M–ZrO_2) and zircon in the same proportions to compositions derived by adding 5%, 10%, 20% and 30% spinel by weight to MgO (M–S–zircon). Chemical analyses of raw materials are given in Table 1. Batches prepared using fine, medium and large sized MgO (0–1 mm), spinel (0–1 mm) and zircon (~13 μm) were shaped into samples of ~8 mm × 8 mm × 60 mm applying ~100 MPa pressure. The samples were sintered for 2 h in kiln (Nabertherm HT16/18) at 1600 °C at 5 °C/min heating and cooling rates. After the surfaces of samples sintered were polished for ~2 min using 800 and 1200 grade SiC paper, mechanical tests were performed after dehydration at ~110 °C in the drying oven.

The mechanical tests, performed using a load cell of 2 kN moving at a velocity of 0.5 mm/min, were applied to minimum 5–6 samples in order to take average values. Bend strength [14] was measured in three point loading with support roller span (L) of 50 mm. Young's modulus (E) was calculated on the basis of the initial, steepest straight-line portion of the load–deflection curve, with correction for machine stiffness [15], using the standard relationship:

$$E_m = \frac{L^3}{4WD^3}m \quad (1)$$

where m is the initial slope of the curve, W is the bar width, and D is the bar thickness. K_{1C} values were calculated by using notches (by single edge notched beam (SENB) method) at a depth of ~25% of thickness of the material using a diamond disk 700 μm thick on specimens using standard equation [16–19]:

$$K_{1C} = \frac{3PL\sqrt{C}}{2WD^2} \quad (2)$$

where Y is given by:

$$Y = A_0 + A_1\left(\frac{c}{D}\right) + A_2\left(\frac{c}{D}\right)^2 + A_3\left(\frac{c}{D}\right)^3 + A_4\left(\frac{c}{D}\right)^4 \quad (3)$$

For $L/D \sim 8$ [18]:

$$A_0 = +1.96, \quad A_1 = -2.75, \quad A_2 = +13.66, \quad A_3 = -23.98, \quad A_4 = +25.22$$

Notch depth was measured using an Olympus BX60M brand optical microscope. SEM studies were carried out using Zeis Evo 50 device to analyze the microstructures and fracture surfaces of materials. Using photographs taken on surfaces of specimens, which were polished and thermally etched for 10 min at 1450 °C, the average MgO grain size was calculated using standard equation employing the linear intersection technique [20]. Bulk density and apparent porosity of bars were measured using the standard water immersion method [21]. X-ray diffraction measurements were carried out using a Rigaku RINT 2000 series set and a Cu Kα X-ray radiation. A scanning speed of 2°/min was used for the 2θ 10–70°.

3. Results and discussion

Based on phase analysis results, MgO and cubic-ZrO_2 were determined in M–ZrO_2 system where forsterite ($2MgO{\cdot}SiO_2$) and cubic-ZrO_2 phases were determined in the M–S–Zircon system beside MgO and $MgAl_2O_4$ phases. Forsterite phase, having a high melting temperature, was formed after reaction of MgO with SiO_2 which was released after decomposition of zircon ($ZrSiO_4$) as SiO_2 and ZrO_2. It was observed that sintering was more effective with the formation of the new phase. The average density values measured for MgO and M–spinel refractories were ~2.8 g/cm^3 going up to ~3.1 g/cm^3 with increasing addition of zircon. Porosity, on the other hand, was ~22% in MgO and M–spinel materials, displaying a reduction trend down to ~14% as the quantity of added zircon was increased. Addition of spinel to MgO had a very little effect on density and porosity, since theorical density of both components was identical (d_{MgO}: 3.583 and d_{spinel}: 3.578) and usage of spinel did not have a promoting effect on sintering. Inclusion of zircon to M–spinel and ZrO_2 to MgO, however, increased density and decreased porosity as a result of pinning effect of ZrO_2 and forsterite formation in the case of M–S–zircon (Fig. 1). Mean grain size of the compositions MgO, M–5S, M–10S and M–5S–20zircon were measured as 67 μm, 40 μm, 38 μm and 27 μm, respectively.

Addition of up to 20% of the spinel to MgO decreased both strength and Young's modulus significantly (75%), as well as toughness. Further additions caused no further loss (Figs. 2–4). During cooling from production temperatures, the large difference in thermal expansion coefficient between MgO (13×10^{-6} °C^{-1}) and spinel (7.6×10^{-6} °C^{-1}) generates very large hoop tensile stress around reinforced particles, causing extensive microcracking [22] (Fig. 5). At a certain temperature, microcracks can only occur when the dispersed particle size is larger than a critical value. MgO–spinel composites with

Table 1
Chemical analysis of raw materials (in wt.%).

	SiO_2	Al_2O_3	MgO	CaO	ZrO_2	Fe_2O_3	HfO_2	Total
MgO (fine)	1.16	0.35	95.61	1.33	–	0.93	–	99.38
MgO (medium–large)	1.00	0.36	95.78	1.25	–	0.93	–	99.32
Spinel (medium–large)	0.44	64.05	34.13	0.54	–	0.53	–	99.69
Zircon	34.23	1.70	–	0.08	62.30	0.15	–	98.46
ZrO_2	0.16	–	–	–	97.87	0.05	1.94	100.02

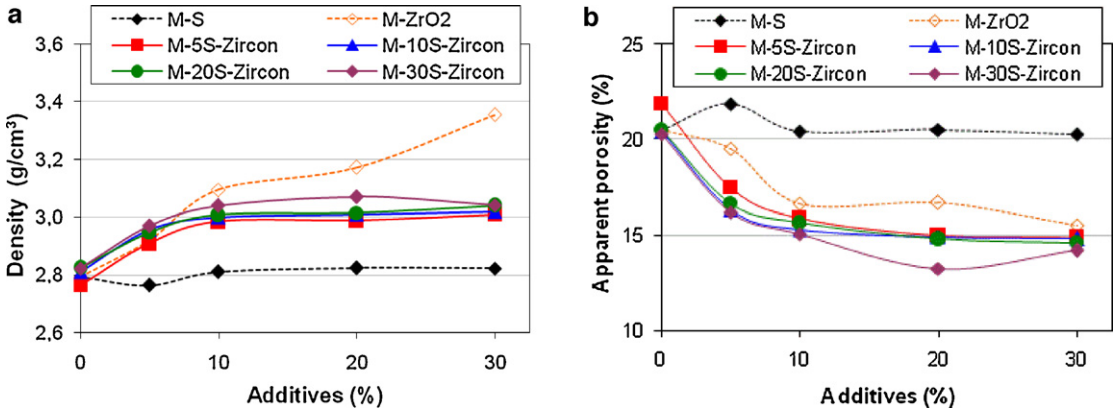

Fig. 1. (a) Density and (b) apparent porosity values as a function of additives.

$\alpha_{spinel} < \alpha_{MgO}$ show low strengths because the radial cracks produced readily link together [23,2,24]. Thermal expansion mismatch between MgO and spinel therefore can lead to a reduction in strength because of an increase in crack length and a decrease in Young's modulus [25–30]. The microcracks decrease the overall strength and stiffness [31,32]. For more than 20% spinel addition, owing to the interlinking of microcracks, no more decrease occurs. Because the mean

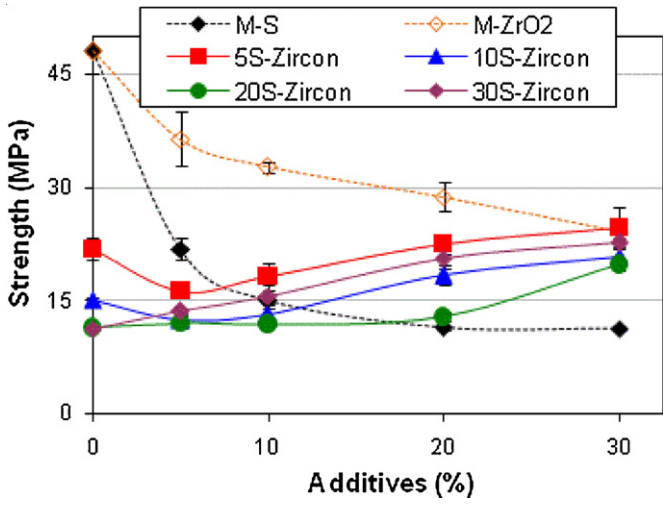

Fig. 2. Strength as a function of additives (M: MgO, S: $MgAl_2O_3$, and Zircon: $ZrSiO_4$).

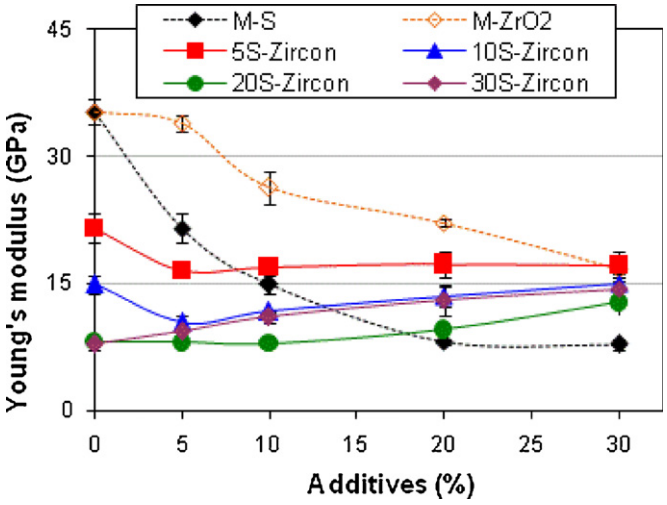

Fig. 3. Young's modulus as a function of additives (M: MgO, S: $MgAl_2O_3$, and Zircon: $ZrSiO_4$).

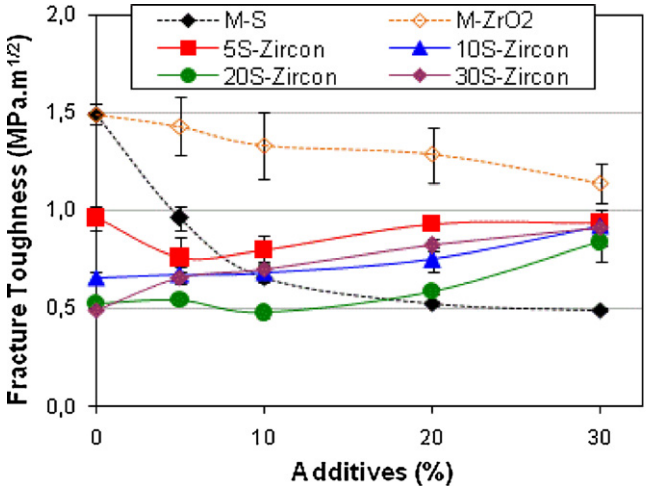

Fig. 4. Fracture toughness as a function of additives (M: MgO, S: $MgAl_2O_3$, and Zircon: $ZrSiO_4$).

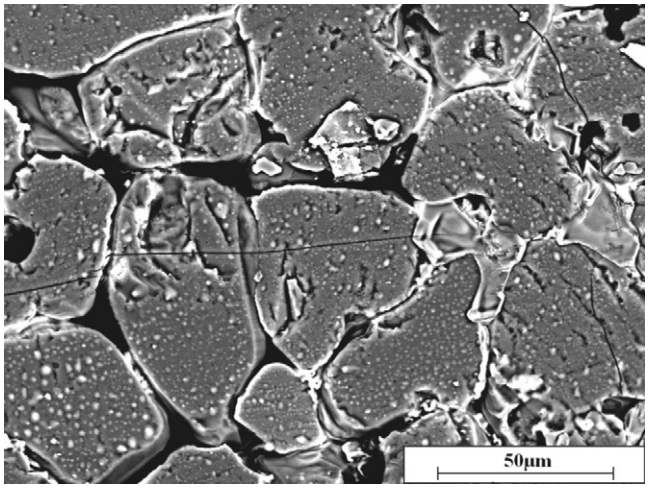

Fig. 5. SEM micrograph showing the microstructure of a M–20spinel composite.

grain size of ZrO_2 is much smaller than spinel, ZrO_2 addition was not as effective as spinel even though the difference in coefficient of thermal expansion is higher than M–spinel. An overall increase was observed in strength with zircon addition as well as in Young's modulus. Among all the compositions, 30% zircon addition gave the highest strength values. Strength of M–30S–30zircon had 2-fold improvement compared to that of M–30spinel.

As ≥10% zircon was added to refractories containing various proportion of spinel, the fracture toughness values of materials basically rose with increasing amount of zircon and they were higher than the fracture toughness of non-additive M–spinel materials. The fracture toughness of all compositions containing 30% zircon were close each other, displaying ∼2-fold improvement compared to non-additive M–spinel (Fig. 4).

It is clear from Fig. 5 that the loss of strength in the composites is not the result of the influence of spinel on magnesia grain size. The observed changes in composite strength with increasing spinel loading are consistent with the generation of microcracks. Direct evidence of microcracking is seen in polished faces, typified by Figs. 5 and 7. These microcracks, it has been assumed, are the result of the large thermal expansion mismatch between the MgO matrix grains and the spinel particles. In fact in very many cases, the

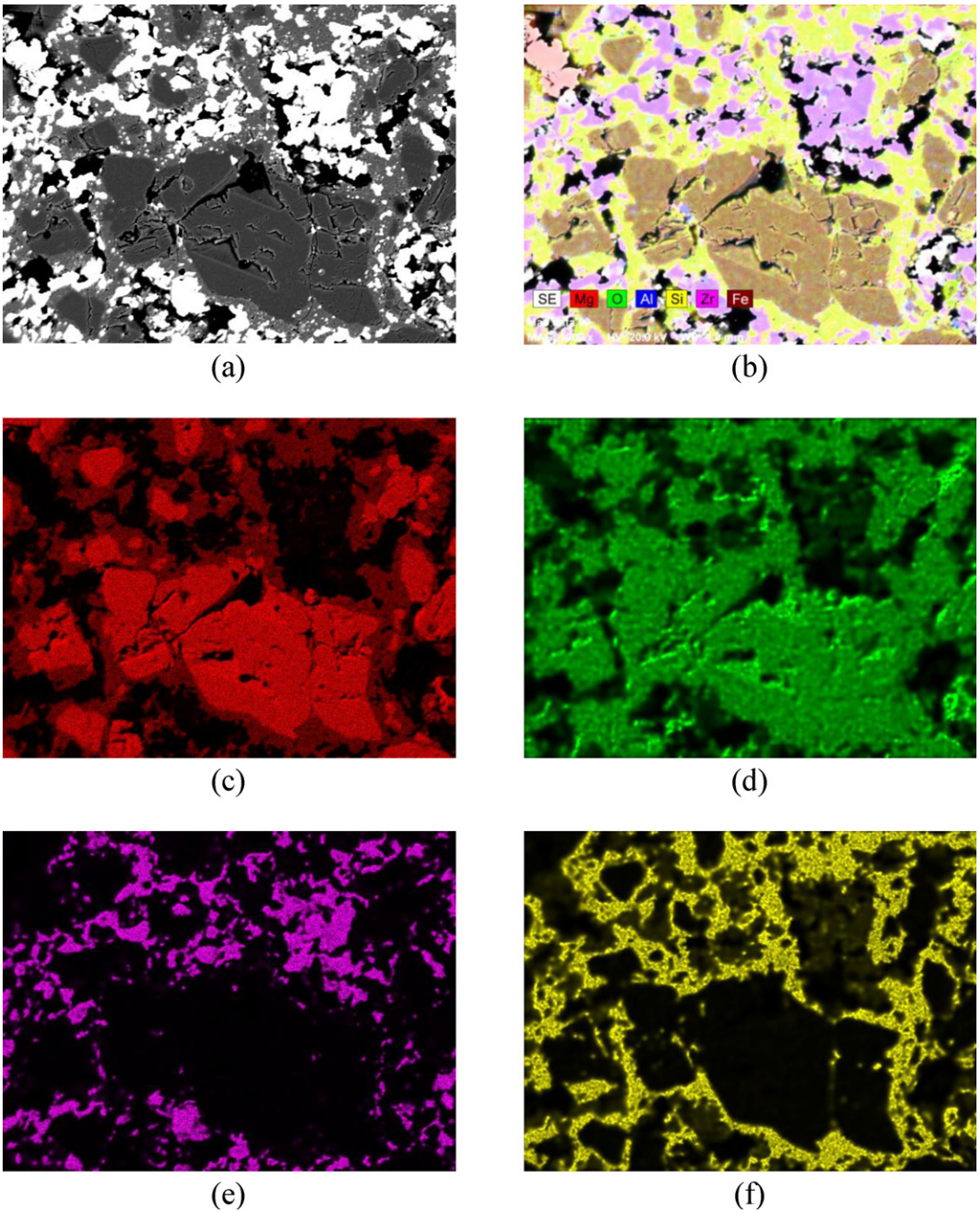

Fig. 6. Electron mapping images of the sample M–20S–20zircon: (a) and (b) general image, (c) Mg, (d) O, (e) Zr, and (f) Si.

intergranular cracking might be more accurately described as grain boundary separation. The microcracking becomes more extensive, the higher the spinel content. Much of the cracking appears to be intergranular, but with the more extensively cracked materials, cracks clearly also extend through MgO grains, following the natural cleavage planes. The decrease in strength of the spinel composites is, therefore, more likely to be related to a decrease of fracture toughness with decreasing E and fracture energy [13,22].

Integration of zircon to MgO–spinel composite refractories has two particular effects: (i) the difference in coefficient of thermal expansion that is effective for compositions including low rate of spinel (i.e. M–5spinel or M–10spinel) causes more microcrack generation when interlinking has not started yet [33,34], and (ii) pinning effect of ZrO_2 inhibits grain growth. Amount of reinforcement has a significant effect on strength both for MgO–spinel and for MgO–spinel–zircon but not as much as SiO_2 which forms forsterite (Mg_2SiO_4) and causes a natural bond between matrix MgO grains (Fig. 6). Even though forsterite brick, without any addition, does not have enough refractivity or corrosion resistance, secondary forsterite formation in basic bricks improves densification and slag leakage resistance through joining matrix grains [35,36].

Since ZrO_2 stays in the cubic form even after cooling, advance in the fracture toughness with zircon addition cannot be associated with transformation toughening of ZrO_2, but the forsterite formation that aids sintering.

The microstructural image of M–5S–20zircon composition is given in Fig. 7. The white colored ZrO_2 grains released as a result of the decomposition of zircon mostly lie in the MgO boundaries. It is observed that the microcracks formed in the structure are connected to each other and progress for a short distance and stop when they reach cubic-ZrO_2 grains or when they reach to the pores.

Fig. 8 shows that for spinel composites, there was no such a fall either in strength or in Young's modulus like for the compositions prepared with more than 10% spinel and zircon. On the other hand, zircon had a little effect on the Young's modulus of the refractory materials with 5% spinel whereas strength declined dramatically, which shows these materials are more sensitive to additives than the others.

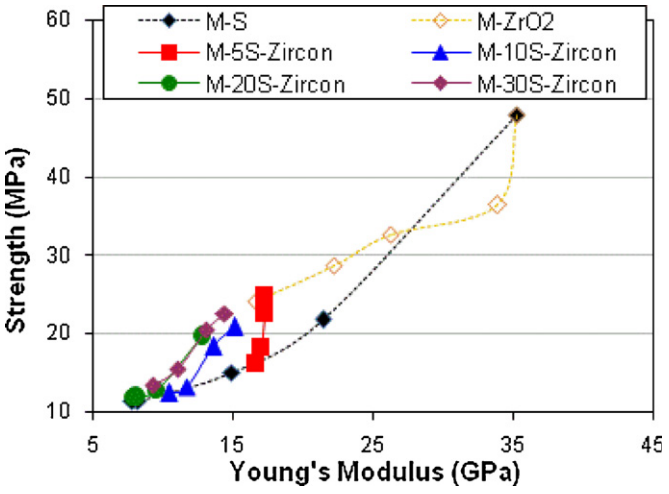

Fig. 8. Strength as function of Young's modulus (M: MgO, S: $MgAl_2O_3$, and Zircon: $ZrSiO_4$).

Fracture surface energy values obtained from modulus and SENB toughness values using the standard relationship:

$$\gamma_i = \frac{K_{IC}^2}{2E} \tag{4}$$

are given in Fig. 9.

Surface energy decreased by ~50% with the additions of spinel up to 10% and values remained almost constant for further additions whereas more than 10% ZrO_2 did not affect the fracture surface energy after 10% increase. As the microcracks, generated during cooling, extended with spinel addition, transgranular fracture faces of pure MgO showed a marked tendency towards intergranular fracture, the tendency being more marked the higher the spinel loading, as illustrated in Fig. 10.

In the case of MgO–spinel–zircon, fracture surface energy of the refractory materials increased with zircon incorporation,

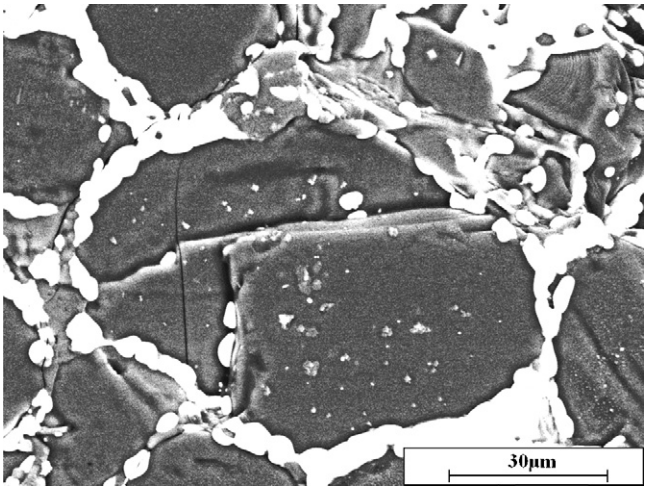

Fig. 7. SEM micrograph showing the microstructure of a M–5S–20zircon composite.

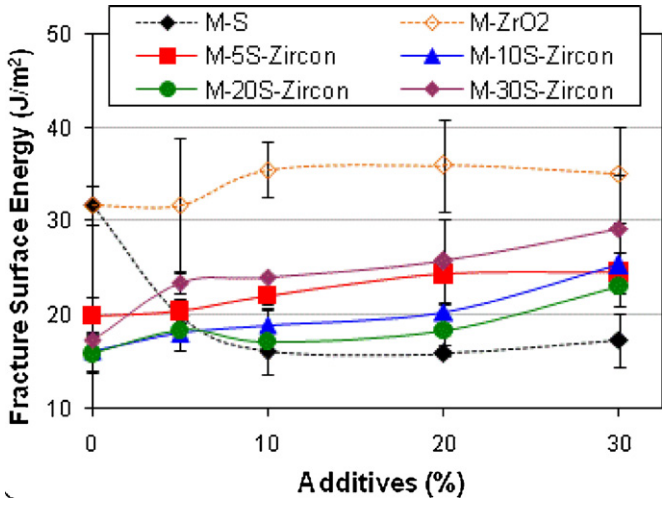

Fig. 9. Fracture surface energy as a function of additives (M: MgO, S: $MgAl_2O_3$, and Zircon: $ZrSiO_4$).

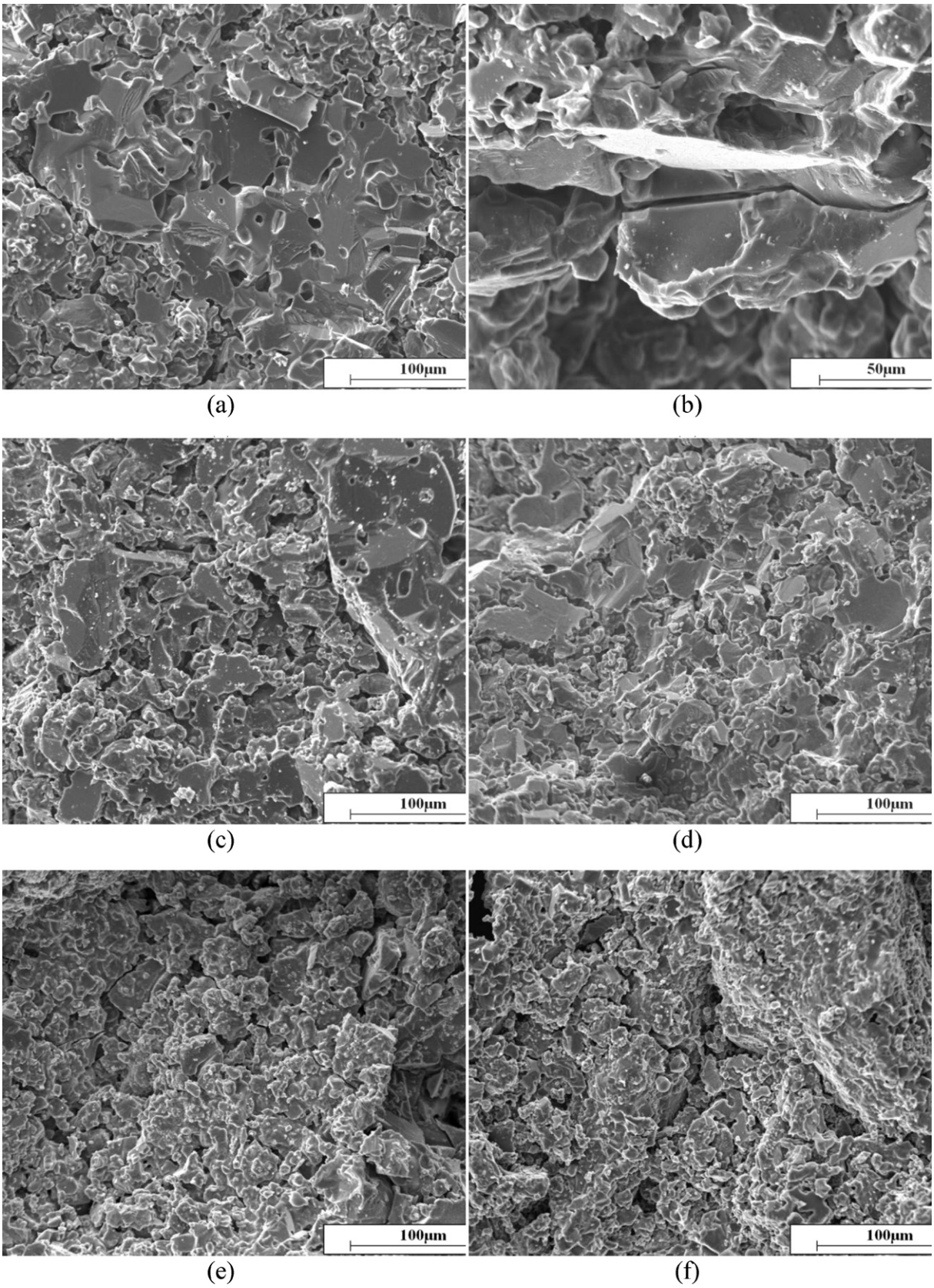

Fig. 10. SEM micrograph of a fracture surface of (a) and (b) pure MgO, (c) M–5spinel, (d) M–10spinel, (e) M–20spinel and (f) M–30spinel.

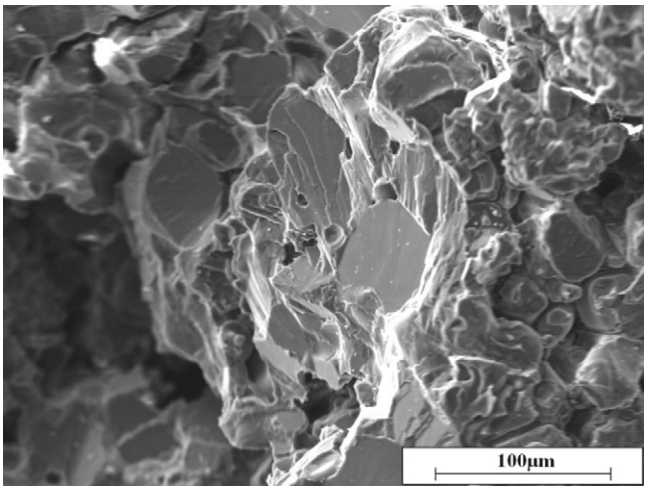

Fig. 11. SEM micrograph of a fracture surface of M–5S–20zircon.

M–30S–30zircon being ~2-fold higher than M–30spinel. Forsterite formation not only caused a natural bonding between matrix particles but also diminished weak zones within the entire material which are basically the source of initiation of fracture propagation. As a result, fracture path turned to transgranular along with defective zones decrease (Fig. 11).

Values for the work of fracture (γ_{WOF}) were calculated from load–deflection curves obtained from notched bars deformed in three-point bend, by measuring the area (U) under the load–deflection curve. γ_{WOF} is given by the following equation [37,38]:

$$\gamma_{WOF} = \frac{U}{2W(D-c)} \quad (5)$$

There was a general increase in γ_{WOF} with increasing spinel content (Fig. 12). Fracture surfaces of pure MgO showed a large proportion of transgranular cracks, with some intergranular cracks (Fig. 10a–d). At low rate additions of spinel, transgranular cracks were still present with some intergranular cracks, in the fracture surfaces of each spinel composite. However, mostly intergranular fracture occurred at higher additions of spinel (20–30%) (Fig. 10e and f). It therefore appears that higher values

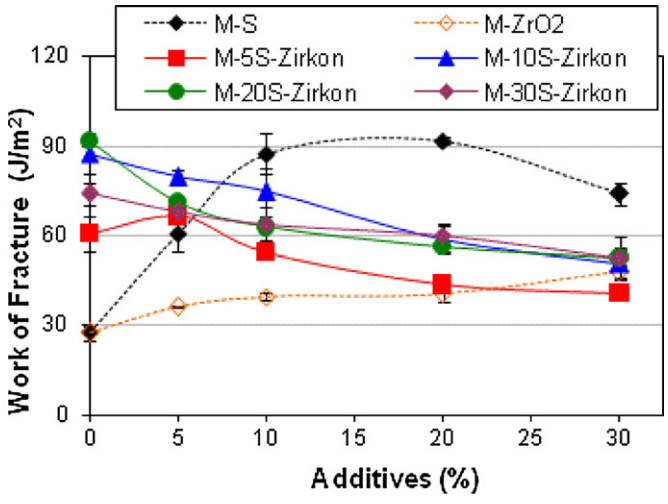

Fig. 12. Work of fracture as a function of additives (M: MgO, S: $MgAl_2O_3$, and Zircon: $ZrSiO_4$).

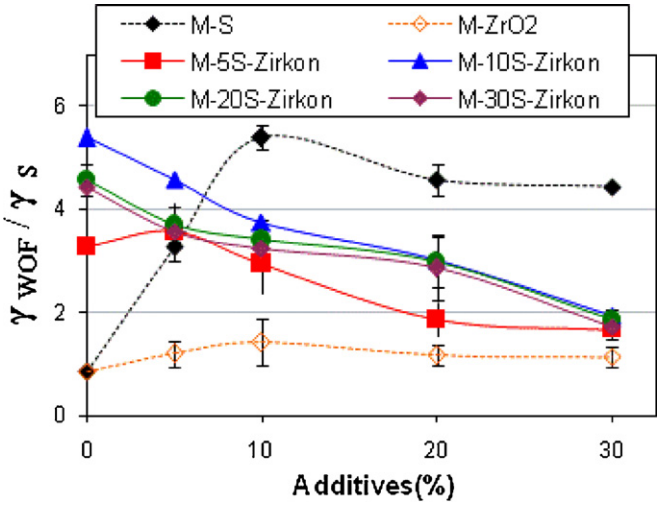

Fig. 13. γ_{WOF}/γ_i ratio as a function of additives (M: MgO, S: $MgAl_2O_3$, and Zircon: $ZrSiO_4$).

of γ_{WOF} are associated with the occurrence of more intergranular fracture with increasing spinel additions. The fracture of the magnesia–spinel composites is either semi-stable or stable, but never catastrophic like MgO. It may be concluded that crack propagation is a much greater energy consuming process than crack initiation in these materials. For many industrial applications, the initiation of fracture is less important than γ_{WOF} and the degree of damage (e.g. further loss of mechanical integrity by strength and material loss through large scale fracture behind the hot face) [39]. Large values of the γ_{WOF}/γ_S ratio were obtained in these composites (Fig. 13). This is a basic requirement for refractory materials to show good thermal shock damage resistance [40]. Fig. 13 illustrates that the M–10spinel composite showed the highest γ_{WOF}/γ_i ratio, by a factor of ~6, as compared to pure MgO. For refractory materials prepared with MgO–ZrO_2. γ_{WOF} values had an increasing trend but not as much as in MgO–spinel owing to the fact that ZrO_2 had much smaller grain size which kept fracture in transgranular form. In the case of M–S–zircon, γ_{WOF} generally decreased with increasing amount of zircon. Forsterite formation, at the grain boundaries, strengthens the microstructure and causes the fracture type to change into transgranular form (Fig. 11). None of the compositions, containing zircon, has as high γ_{WOF} as M–spinel. On the other hand, even these materials could have high thermal shock resistance due the fact that they have higher resistance to fracture initiation.

4. Conclusions

Cubic-ZrO_2 and forsterite were detected in MgO–spinel–zircon refractories accompanied with the matrix periclase and spinel. Mechanical properties of MgO–spinel refractories deteriorated with the increasing amount of spinel up to 20% and higher loads caused no more damage, for which MgO–ZrO_2 refractories showed the same trend but not as effective as MgO–spinel. With the addition of zircon, both strength and Young's modulus as well as fracture toughness and fracture surface energy increased for almost 2 times higher than MgO–spinel composite refractories with the aid of forsterite formation which formed a natural bonding

between matrix grains. Forsterite formation not only increased the mechanical properties but also caused the fracture path to change into transgranular form which is an indicator of resistance to fracture initiation, but caused γ_{WOF} to be decreased.

Acknowledgements

This study was partly supported by Anadolu University and in part TÜBİTAK project 106M394 with partial support provided also by Konya Selçuklu Krom Magnezit Tuğla Sanayi A.Ş.

References

[1] P. Bartha, H.J. Klischat, Present state of the refractory lining for cement kilns, CN-Refractories 6 (3) (1999) 31–38.
[2] W. Tabbert, H.J. Klischat, Magnesia spinel bricks for the cement industry, in: Proceedings Beijing China Symposium, China, (1992), pp. 424–430.
[3] M. Kuennecke, K. Wieland, M. Faizullah, The correlation between burning zone linings and operation of cement rotary kilns, World Cement (Part 2) (1986) 247–253.
[4] P. Bartha, Magnesia spinel bricks—properties, production and use, in: X. Zhong, al. et (Eds.), Proc. Int. Symp. Refractories, Refractory Raw Materials and High Performance Refractory Products, Pergamon, Hangzhou, (1989), pp. 661–674.
[5] J.A. Reyes Sanchez, O.D. Toledo, New developments of magnesite–chrome brick and magnesite–spinel for cement rotary kilns higher thermal shock resistance and higher coating adherence, in: Proc. UNITECR 89, Anaheim, USA, (1989), pp. 968–979.
[6] R. Dal Maschio, B. Fabbri, C. Fiori, Industrial applications of refractories containing magnesium aluminate spinel, Ind. Ceram. 8 (3) (1988) 121–126.
[7] G.E. Gonsalves, A.K. Duarte, P.O.R.C. Brant, Magnesia-spinel brick for cement rotary kilns, Am. Ceram. Soc. Bull. 72 (2) (1993) 49–54.
[8] S.E. Laurich-McIntyre, R.C. Bradt, Room temperature strengths of individual tabular alumina and sintered spinel grains (aggregates), in: UNITECR'93 Congress, Sao Paulo, Brazil, 1993.
[9] H.J. Klischat, Refractory lining review for cement kiln system, ZKG Int. 58 (2) (2005) 33–45.
[10] D.R. Wilson, R.M. Evans, I. Wadsworth, J. Cawley, Properties and applications of sintered magnesia alumina spinels, in: UNITECR'93 Congress, Sao Paulo, Brazil, (1993), pp. 749–760.
[11] M. Kimura, Y. Yasuda, H. Nishio, Development of magnesia spinel bricks for rotary cement kilns in Japan, in: Proc. 26th Int. Col. Ref. Interceram Special Issue, vol. 33, Aachen, Germany, (1983), pp. 344–376.
[12] S.C. Cooper, T.A. Hudson, Magnesia–magnesium aluminate spinel as a refractory, Trans. J. Br. Ceram Soc. 81 (4) (1982) 121–128.
[13] C. Aksel, F.L. Riley, Effect of the particle size distribution of spinel on the mechanical properties and thermal shock performance of MgO–spinel, J. Eur. Ceram. Soc. 23 (2003) 3079–3087.
[14] G.A. Rankin, H.E. Merwin, Ternary system CaO–Al_2O_3–MgO, J. Am. Chem. Soc. 38 (3) (1916) 568–588;
Standard test methods for flexural strength of advanced ceramics at ambient temperature, Annual Book of ASTM Standards, Designation: C1161-90, 15.01 1991, pp. 327–333.
[15] Standard test methods for flexural properties of unreinforced and reinforced plastics and electrical insulating materials, Annual Book of ASTM Standards, Designation: D790M-86, 08.01 1988, pp. 290–298;
I. Ganesh, S. Bhattacharjee, B.P. Saha, R. Johnson, K. Rajeshwari, R. Sengupta, M.V. Ramanarao, Y.R. Mahajan, An efficient $MgAl_2O_4$ spinel additive for improved slag erosion and penetration resistance of high-Al_2O_3 and MgO–C refractories, Ceram. Int. 28 (2002) 245–253.
[16] D.R. Larson, J.A. Coppola, D.P.H. Hasselman, R.C. Bradt, Fracture toughness and spalling behaviour of high-Al_2O_3 refractories, J. Am. Ceram. Soc. 57 (10) (1974) 17–421.
[17] Standard test method for plane-strain fracture toughness of metallic materials, Annual Book of ASTM Standards, Designation: E399-90, 03.01 1991, pp. 485–515.
[18] Standard test methods for plane-strain fracture toughness and strain energy release rate of plastic materials, Annual Book of ASTM Standards, Designation: D5045-91, 08.03 1991, pp. 728–736.
[19] W.F. Brown, J.E. Srawley, Plane Strain Crack Toughness Testing of High Strength Metallic Materials, ASTM Special Technical Publication, vol. 410, 1967.
[20] M.I. Mendelso n, Average grain size in polycrystalline ceramics, J. Am. Ceram. Soc. 52 (1969) 443–446.
[21] British Standard Testing of Engineering Ceramics, BS 7134 Section 1.2, 1989.
[22] C. Aksel, R.W. Davidge, P. Knott, F.L. Riley, Mechanical properties of magnesia-magnesium aluminate spinel composites, in: III Ceramic Congress Proceedings Book. Engineering Ceramics, vol. 2, Istanbul, Turkey, (1996), pp. 172–179.
[23] C. Aksel, P.D. Warren, Work of fracture and fracture surface energy of magnesia–spinel composites, Compos. Sci. Technol. 63 (10) (2003) 1433–1440.
[24] C. Aksel, R.W. Davidge, P.D. Warren, F.L. Riley, Investigation of thermal shock resistance in model magnesia–spinel refractory materials, in: IV. Ceramic Congress, Proceedings Book, Part 1, Eskisehir, Turkey, (1998), pp. 193–199.
[25] R.W. Davidge, Mechanical Behaviour of Ceramics, Cambridge University Press, Cambridge, 1979.
[26] C. Aksel, R.W. Davidge, P.D. Warren, F.L. Riley, Mechanical properties of model magnesia–spinel composite materials, in: In Euro Ceramics V, Part 3, Extended Abstracts of the 5th Conference and Exhibition of the European Ceramic Society—Key Engineering Materials, vols. 132–136, Versailles, France, (1997), pp. 1774–1777.
[27] R.V. Mastelaro, E.D. Zanotto, Residual stresses in a soda lime–silica glass-ceramic, J. Non-Cryst. Solids 194 (1996) 297–304.
[28] Thermal shock behaviour and mechanical properties of magnesia–spinel composites, Ph.D. Thesis, Department of Materials Engineering, University of Leeds, Leeds, UK, 1998.
[29] C. Aksel, P.D. Warren, F.L. Riley, Fracture behavior of magnesia and magnesia–spinel composites before and after thermal shock, J. Eur. Ceram. Soc. 24 (8) (2004) 2407–2416.
[30] C. Aksel, B. Rand, F.L. Riley, P.D. Warren, Thermal shock behavior of magnesia–spinel composites, J. Eur. Ceram. Soc. 24 (9) (2004) 2839–2845.
[31] C. Aksel, B. Rand, F.L. Riley, P.D. Warren, Mechanical properties of magnesia–spinel composites, J. Eur. Ceram. Soc. 22 (5) (2002) 745–754.
[32] F. Simonin, C. Olagnon, S. Maximilien, G. Fantozzi, L.A. Díaz, R. Torrecillas, Thermomechanical behavior of high-alumina refractory castables with synthetic spinel additions, J. Am. Ceram. Soc. 83 (10) (2000) 2481–2490.
[33] A. Ghosh, R. Sarkar, B. Mukherjee, S.K. Das, Effect of spinel content on the properties of magnesia–spinel composite refractory, J. Eur. Ceram. Soc. 24 (2004) 2079–2085.
[34] V.I. Shubin, V. Sakulin, V.P. Migal, S.I. Gershkovich, A.P. Margishvili, V.V. Bulin, Choosing functional additives for optimizing the properties of periclase–spinel composites, Refract. Ind. Ceram. 48 (1) (2007) 69–72.
[35] Refractories Handbook, The Technical Association of Refractories, Japan, 1998.
[36] A.G.M. Othman, N.M. Khalil, Sintering of magnesia refractories through the formation of periclase–forsterite–spinel phases, Ceram. Int. 31 (2005) 1117–1121.
[37] R.W. Davidge, G. Tappin, The effective surface energy of brittle materials, J. Mater. Sci. 3 (33) (1967) 165–173.
[38] J.A. Coppola, D.P.H. Hasselman, R.C. Bradt, On the measurement of the work-of-fracture of refractories, Am. Ceram. Soc. Bull. 17 (1972) 578.
[39] D.P.H. Hasselman, Strength behaviour of polycrystalline alumina subjected to thermal shock, J. Am. Ceram. Soc. 53 (1970) 490–495.
[40] J. Nakayama, H. Abe, R.C. Bradt, Crack stability in the work-of-fracture test: refractories applications, J. Am. Ceram. Soc. 64 (1981) 671–675.